ELSEVIER

Surface Science 396 (1998) 411–421

surface science

Photoemission electron microscopy of Schottky contacts

Margret Giesen [a,*], Raymond J. Phaneuf [a,b], Ellen D. Williams [a], Theodore L. Einstein [a]

[a] *Department of Physics, University of Maryland, College Park, MD 20742-4111, USA*
[b] *Laboratory for Physical Science, University of Maryland, College Park, MD 20740, USA*

Received 6 May 1997; accepted for publication 19 August 1997

Abstract

We demonstrate a new application of photoemission electron microscopy (PEEM) for the investigation of Schottky contacts. As an example we have investigated the changes in contrast in PEEM images when silver is deposited on a lateral p–n diode structure on a Si(100) surface. In agreement with recent studies by other groups, we find three-dimensional island growth in the multilayer regime at low temperatures when silver is grown on the clean silicon surface. We also find three-dimensional growth when silver is deposited on a thin, wet chemically formed oxide layer. In both cases, the p-doped regions appear brighter than the n-doped regions in the PEEM image. When the silver layer is heated to 900°C the islands disappear. For the case of silver on the oxide-free Si(100) surface, the p regions remain brighter than the n regions. In the case of silver growth on an intermediate oxide layer, the contrast in the image changes dramatically during heating. The experimental results are interpreted in terms of the band bending caused by interface states. © 1998 Elsevier Science B.V.

Keywords: Electron emission measurements; Metal–semiconductor interfaces; Polycrystalline thin films; Semiconductor–insulator interfaces; Silicon; Surface electronic phenomena (work function, surface potential, surface states, etc.)

1. Introduction

Recently, we introduced the use of PEEM as a method to provide real-time observations of changes in surface states of silicon two-dimensional p–n junctions [1]. In PEEM images of a device structure, the image contrast arises from different photoemission yields from differently doped areas on the sample when the Fermi level is pinned at the surface by surface states. Due to the pinning, the band bending near the surface depends on the doping, leading to a spatial variation of the effective photo-threshold [1,2]. Hence, changes in the band bending due to structural changes of the surface are indicated by changes in the contrast in PEEM images. In this work, we apply the method to study metal-induced gap states and the Schottky barrier of the silver–silicon contact of a Si(100) device structure as a function of the temperature and as a function of the interface nature. We have deposited silver on the silicon devices under two different surface conditions. In one case silver was grown on a thin oxide layer which remained from the wet etching procedures during sample preparation. In the other cases, the oxide layer was thermally desorbed before silver deposition.

The growth of silver on Si(111) and (100) substrates [3–16] as well as on silicon device structures [17] has attracted considerable interest. Previous investigations have been performed using imaging techniques like tunneling microscopy

* Corresponding author. Fax: (+49) 2461 613907; e-mail: m.giesen@fz.juelich.de

0039-6028/98/$19.00 © 1998 Elsevier Science B.V. All rights reserved.
PII S0039-6028(97)00696-1

(STM) [11–13] and electron microscopy (SEM, TEM, REM) [15,16] as well as diffraction techniques like low-energy electron diffraction (LEED) [6,8]. Schottky barriers and the electronic properties of the metal–semiconductor contact have been studied theoretically using photoemission spectroscopy and by measuring the current–voltage characteristics [16–18].

Previous investigations have established that the growth of silver on Si(100) is two-dimensional up to one monolayer [11,12,14,19]. The silver atoms fill the space between the dimer rows which form the (2×1) reconstruction of the (100) surface plane. For higher coverages, the silver atoms nucleate in large three-dimensional islands. Investigations by Ichinokawa et al. [21] have shown that these islands are mobile due to both thermal diffusion and drift under the influence of an electric field.

In contrast to gold, copper or nickel, there is almost no intermixing between silver and silicon at the interface. The bulk eutectic temperature of this system is about 850°C. Therefore, the interface at this metal–semiconductor contact is sharp and provides an ideal system to study interfacial structure and electronic properties. The aforementioned studies concentrated on two growth conditions of the silver layer, i.e. room-temperature growth and deposition at around 400–500°C. To our knowledge, the structure and the Schottky barrier of the Ag–Si contact formed near the eutectic phase transition has not yet been investigated. In this paper we present PEEM studies of the Ag–Si contact at room temperature and after annealing to 900°C.

The paper is organized as follows. In Section 2 the experimental set-up and the sample preparation are described. In Section 3 the PEEM images and their analysis are presented. We discuss the results in Section 4. We conclude with a summary in Section 5.

2. Experimental

The experiments were performed in a standard UHV chamber with a base pressure in the low 10^{-10} mbar range. The chamber is equipped with a STAIB photoemission electron microscope (PEEM-150). We have determined the resolution of our system to be 0.2 μm. As a UV source we used a short-arc mercury lamp (PTI A1010) whose highest transmitted energy line has its maximum intensity at 4.96 eV. For structural analysis, the chamber was also equipped with a Varian four-grid visual low-energy electron diffraction (LEED) system.

For the silver deposition we used a self-calibrating electron beam evaporator (Omicron EMF 3) which was carefully degassed before each experiment. The deposition rate was determined by the measured flux current. The flux was calibrated by Auger measurements in a different chamber and has been corrected for the different geometry in our chamber. During the silver deposition, the pressure did not exceed 1×10^{-9} mbar.

The sample device was fabricated by boron-ion implantation into a commercial n-doped Si (100) wafer ($N_D=10^{14}$ cm^{-3}), creating a lateral p–n diode array with p^+-doped stripes ($N_A=10^{18}$ cm^{-3}) [22]. The detailed fabrication procedure of the sample device and a sketch of the p–n device have been published elsewhere [1]. Prior to mounting the sample in the chamber, the devices were cleaned and the native surface oxide was removed by Shiraki cleaning [23]. Typically, after the last step of the Shiraki cleaning the sample is covered by a thin hydrophilic oxide which can be sublimated off by heating in vacuum to temperatures of 600–700°C. The sample was mounted to the sample holder and brought into a pre-vacuum of 10^{-3} mbar within 15 min of the last etching step. The pressure decreased to 10^{-6} mbar within an additional 20–30 min. After a typical bakeout of 24 h, no contamination-associated features were resolvable in the PEEM images and the LEED pattern displayed a diffuse (2×1) structure. In the case of silver deposition on the bare silicon surface, the thin oxide remaining from the etching procedure was removed by heating to 800°C several minutes before the silver was deposited on the device structure. In all experiments, the silver was deposited exclusively at room temperature.

The images were displayed on a multichannel plate (MCP) installed in the PEEM and imaged

through a view port by an SIT Vidicon video camera. For later analysis, the images were simultaneously stored on a video tape. Fig. 1 shows a PEEM image of a freshly prepared sample after the bakeout when the thin etch-oxide layer still remains on the surface. The array of parallel bright and dark stripes correspond to p- and n-doped areas in the parallel diode structure, respectively [1]. The distance between the bright p stripes is about 30 μm. Their apparent width is approximately 3 μm. This image corresponds to a single frame grabbed from the video tape. For the detailed intensity profile analysis of the images we used a digitizing frame averager which is capable of averaging up to 128 single frames and displaying the result continuously.

3. Results

3.1. Silver deposition on the Shiraki oxide

We first present the results obtained from the deposition of silver on the Shiraki oxide layer. Fig. 2 shows a PEEM image from the surface after silver deposition at room temperature. The coverage is about 7 ML ($1\ ML = 7.8 \times 10^{14}$ atoms cm^{-2}). The deposition rate was $0.2\ ML\ s^{-1}$. The bright spots in the image correspond to large three-dimensional islands on the diode structure. Here, the top of these islands lie in the object plane of the PEEM, and therefore the array of the diode structure is not well resolved. Island nucleation occurs on both p- and n-doped regions. However, the nucleation probability seems to be higher on the bright p stripes since most of the islands nucleate on top of the p stripes.

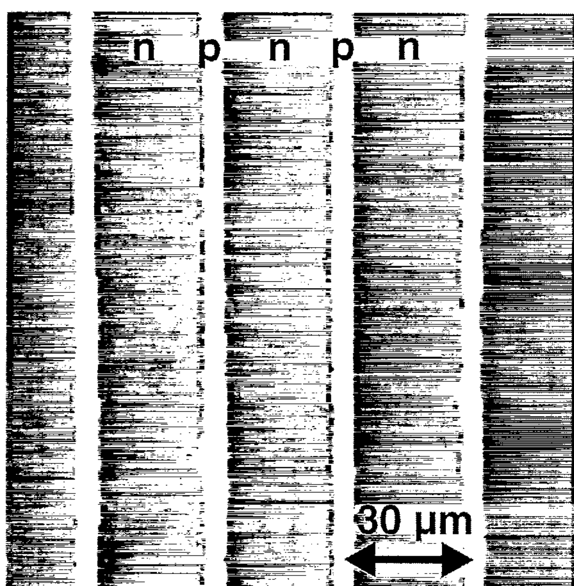

Fig. 1. PEEM image of the lateral diode structure after Shiraki cleaning.

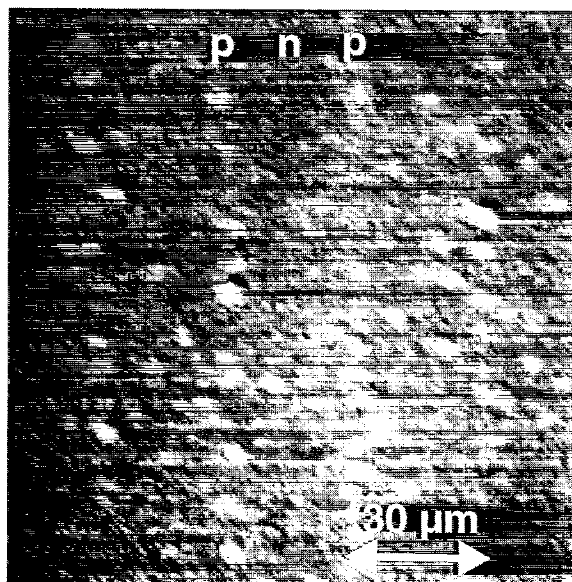

Fig. 2. PEEM image of the sample after 7 ML growth (growth rate = $0.2\ ML\ s^{-1}$) of silver on the Shiraki oxide layer at room temperature. The image is focused on the three-dimensional islands, and therefore the lateral diode structure is poorly resolved.

In Fig. 3 a sequence of PEEM images is displayed, showing the development of the image contrast of a sample like that shown in Fig. 2 upon radiative heating to 700°C. With increasing temperature, the overall intensity of the PEEM image decreases. This decrease is accompanied by a decrease in contrast between the islands and the background (Fig. 3b). The decrease in contrast between p and n upon annealing is due to the temperature dependence of the position of the bands relative to the Fermi level. Upon heating, the bands shift so that the Fermi level is positioned

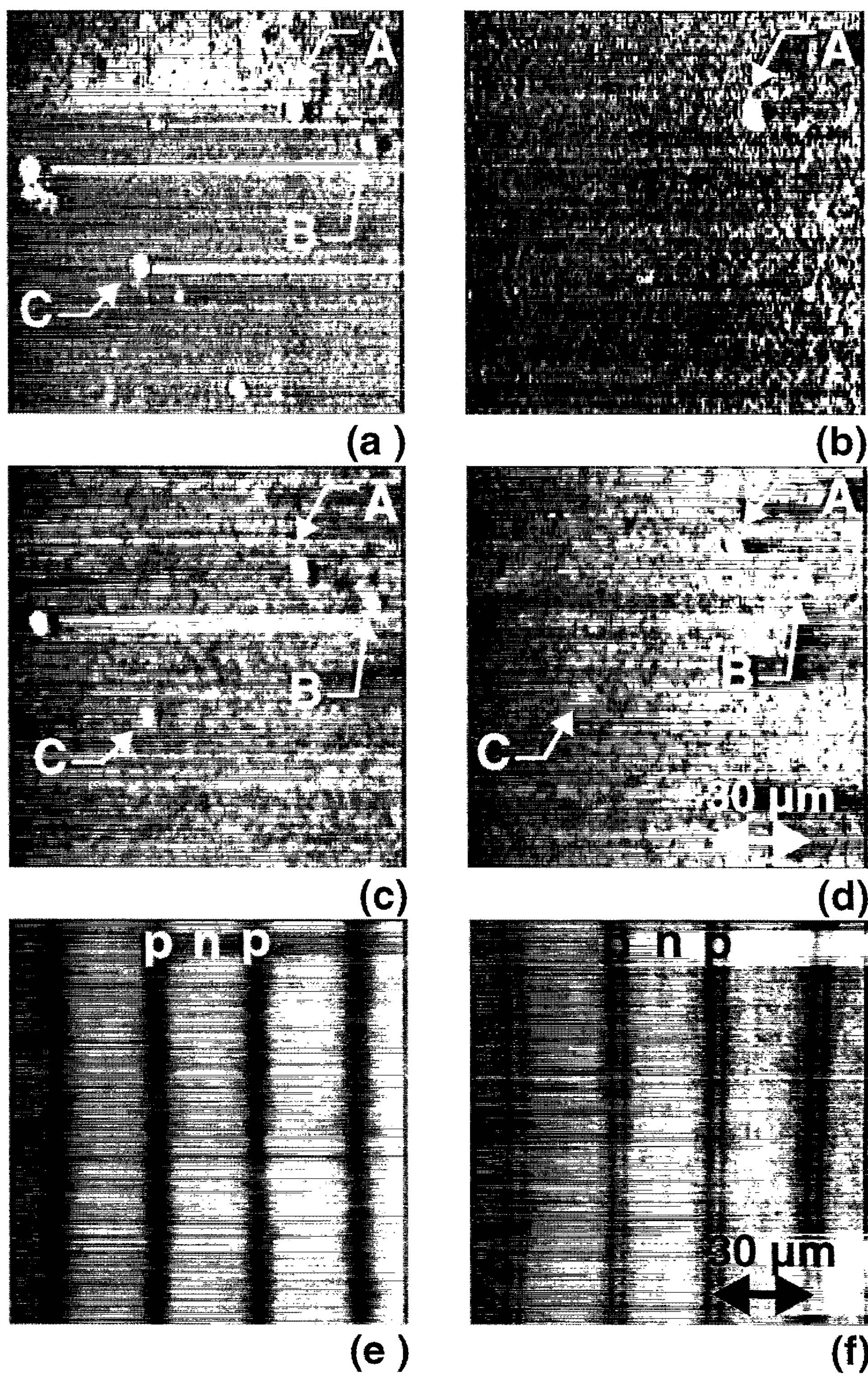

Fig. 3. Annealing of the sample in Fig. 2: (a) 300°C, (b) 700°C, (c) after cooling to 300°C, (d) sample after three annealing/cooling steps to 700/300°C, respectively, (e) after further annealing to 900°C for several seconds, (f) after cooling to room temperature.

nearly in the middle of the band gap in both doping regions. When the contrast was almost completely lost, the radiative heating was stopped and the sample temperature was decreased again (Fig. 3c). Immediately, islands became visible again (B and C in Fig. 3c). However, the island density was lower. Smaller islands vanished with the first heating step, whereas the larger islands remained visible after prolonged heating at elevated temperatures. No nucleation of new islands occurred after each heating, and all remaining islands appeared at the same position when the sample was cooled. Fig. 3d shows the remaining islands (A, B and C) after three heating/cooling steps. When heating this sample to 900°C for several seconds, most islands disappeared and the p- and n-doped regions of the diode structure became clearly visible, but with reversed contrast compared to Fig. 1. Fig. 3e shows the sample at 900°C after annealing. The p regions appear dark and the n regions are bright. The brightness of the n regions increased dramatically when the sample was then cooled to room temperature (Fig. 3f). In addition, a pronounced intensity maximum developed in the p-doped stripe which was not observed at higher temperature. Fig. 4a shows an image of the same sample as observed after the temperature was decreased to room temperature. Obviously, the dark p area has a small intensity maximum in the center (the extension of the different doping areas is marked by arrows). The image contrast is qualitatively different from either the oxidized surface without silver or the oxide-free surface with silver deposited (see Fig. 6c). In Fig. 4b the intensity profile perpendicular to the p–n stripes is shown as a function of the distance perpendicular to the p stripes (solid curve). The length scales in both Fig. 4a and b are the same.

After heating to 900°C, the island density decreased dramatically. However, some islands were still visible on the surface. They were larger and their shape was more regular compared to the islands before heating to 900°C. Fig. 5 shows PEEM images of the sample shown in Figs. 3f and 4a at different areas on the silicon device. Note in the following images that the scale of the image and hence the size of the islands can be judged by

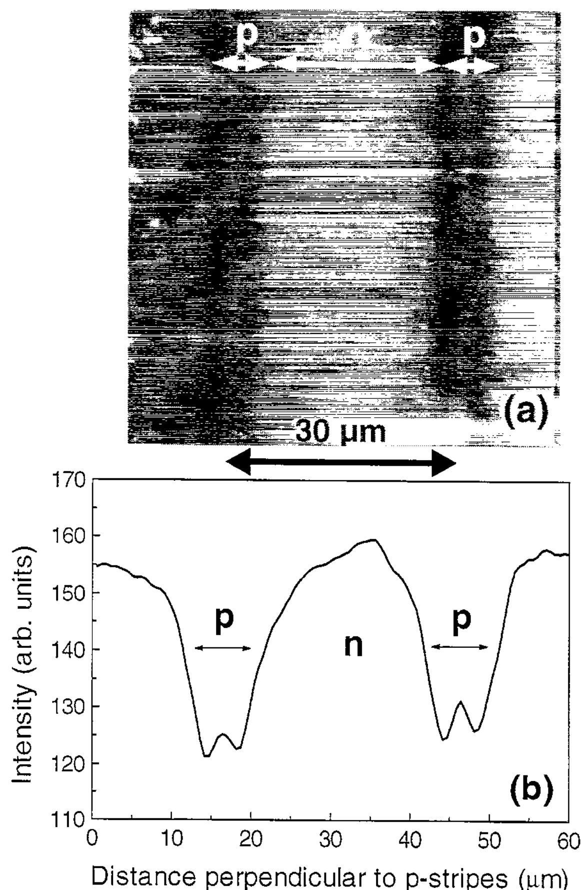

Fig. 4. (a) Section of the image in Fig. 3f. (b) Intensity profile of (a) perpendicular to the lateral diode structure.

the distance between p-doped regions, which is 30 μm. All of the islands in these images have diameters of approximately 10–20 μm. Fig. 5a shows an irregular island nucleated on the n region. In Fig. 5b a large pyramidal island is formed on top of a p stripe. Similarly shaped islands were also observed in STM investigations by Samsavar et al. [11] after deposition of silver on clean Si(100). The dark region displayed on the lower side of the island represents the shadow of the grazing-incidence UV light caused by the island itself. Fig. 5c shows a hexagonal island, also nucleated on top of the p-doped stripe. Here, additional nucleation sites are visible on top of the island. Both the hexagonal island and the topmost nucle-

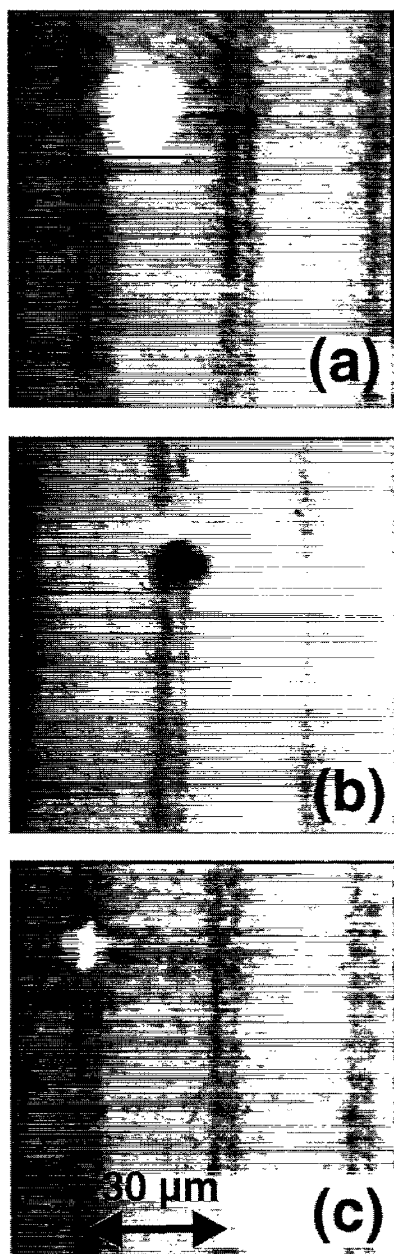

Fig. 5. Remaining islands on the sample of Fig. 3f. (a) Large island with irregular shape (diameter 20 μm). (b) Island with pyramidal shape. Note the shadowing effect on the lower side of the three-dimensional island. The UV source is located on top with respect to the image orientation. (c) Hexagonal island with additional nucleation sites on top.

ation sites have nucleated symmetrically with respect to the center intensity maximum in the dark p region. After the heating to 900°C and subsequent cooling, the LEED pattern showed a diffuse (2×1)-reconstructed surface.

3.2. *Silver deposition on the oxide-free diode structure*

We now present the results obtained for silver deposition on the diode structure after the sample was heated to 800°C to remove the light oxide. Before heating we imaged the sample using the PEEM and found no indication of contamination. The image is shown in Fig. 1. This also allowed us to adjust the object plane of the PEEM to be coincident with the diode structure. Then the sample was heated resistively under the same imaging conditions. Fig. 6a shows the sample after the oxide has been removed by heating the sample to 800°C. Even after cooling to room temperature, no emission was observed. This indicates that the surface electron barrier increases after oxide removal, such that the maximum photon energy available from our mercury lamp is below the photo-threshold over the range of the doping levels of our device [1]. However, we cannot exclude the possibility that along with the increase in the surface barrier, the band bending is changed upon annealing. After the deposition of silver (work function $\phi=4.8$ eV [24]) the electron barrier of the sample is reduced and the contrast of the p–n diode structure is restored (Fig. 6b). After heating the surface further to 900°C, the islands disappeared and the absolute intensity and the contrast increased, with the p-doped stripes remaining brighter than the n-doped areas (Fig. 6c). Fig. 7 shows a line profile measured perpendicular to the p stripes after heating. The intensity profile displays only single maxima and minima in the p- and n-doped regions, respectively. No additional minima are evident in the transition regions between p and n, in contrast to the images obtained for a Shiraki oxide-covered surface without silver [1]. We did not measure the LEED pattern of this surface due to a malfunction of the LEED system.

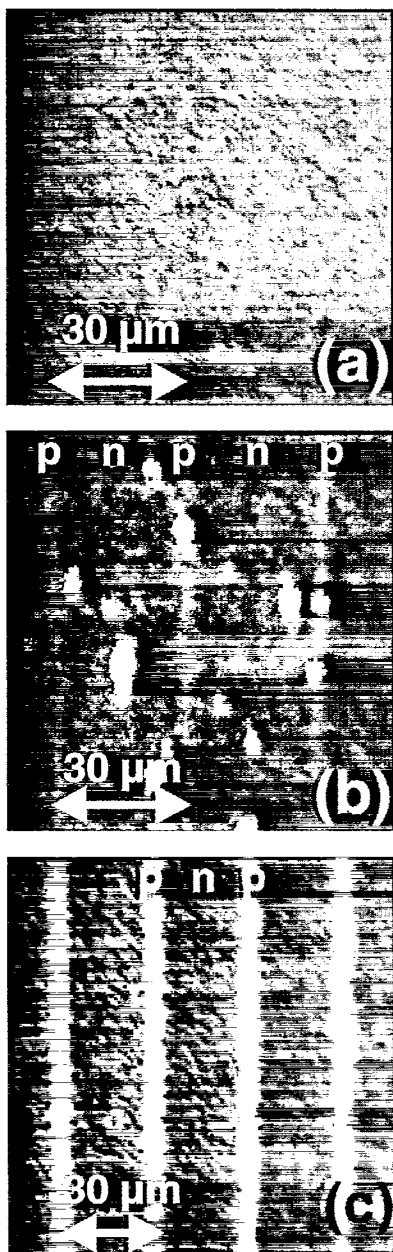

Fig. 6. (a) Clean silicon surface with a lateral diode structure after the Shiraki oxide has been flashed off at 800°C. (b) The same sample as in (a) after deposition of 10 ML silver at room temperature (growth rate = 0.2 ML s^{-1}). (c) The same sample as in (b) after annealing to 900°C for several seconds.

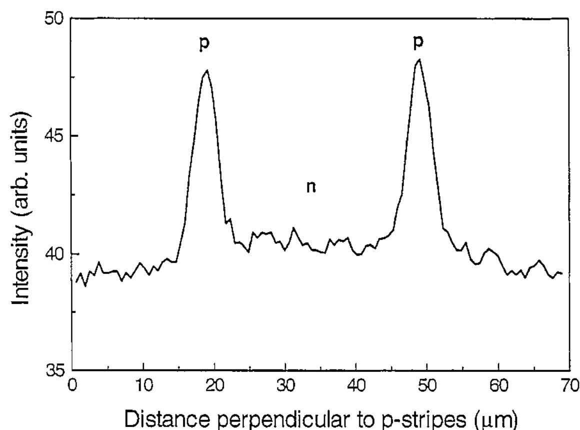

Fig. 7. Intensity profile of Fig. 6c perpendicular to the lateral diode structure.

4. Discussion

4.1. Island growth

For multilayer doses of silver on the device structure, we observed three-dimensional island growth for the deposition of silver on the oxide as well as for the deposition on the bare silicon substrate. The island density at room temperature is in agreement with the studies of other groups [10,12,20]. In many of our PEEM images, the islands nucleated with a higher probability on the p-doped stripes. STM and AFM images of our p–n devices show parallel grooves along the edges of the p stripes with a depth and a width of approximately 5 nm and 1 μm, respectively. We have determined that these grooves are caused by the mask-etching process during device fabrication [25]. These topographic structures may serve as nucleation centers during the deposition of Ag. Our result is similar to studies by Hanbücken et al., who investigated the influence of surface defects on the island nucleation [10]. In those studies, a silicon surface with parallel grooves was used. It was found that the influence of these grooves on nucleation was not dramatic. However, the islands appeared to nucleate preferentially at those defects.

The changing visibility of the islands upon heating and quick cooling can be attributed to two effects. One effect is the change in imaging condi-

tions of the surface in PEEM during annealing, while the other is the sublimation of the silver islands. The image contrast in PEEM is very sensitive to changes in the imaging conditions. When the sample is heated, thermal drifts shift the surface area out of the focal plane of the PEEM and the contrast between the islands and the background is lost. This interpretation is supported by the fact that the islands reappeared at their former sites when the sample was cooled quickly. When the sample was annealed to higher temperatures or for a longer period of time, most of the islands vanished irreversibly. The decrease in the island density for increasing temperature is in agreement with the measurements of Hanbücken et al. in the temperature range 500–900 K [10]. Based on the change in image contrast between the p- and n-doped regions from the clean or the oxidized Ag-free surface, we conclude that some silver is still present on the surface as a homogeneous layer (homogeneous on the resolution scale of the PEEM, which is about 0.2 μm). The assumption of remaining traces of silver and/or oxide after short annealing to 900°C provides a reasonable basis to explain the change in image contrast. In the clean Ag/Si(100) case a complete desorption of silver would lead to a clean Si(100) surface. Hence, one would expect to observe PEEM images such as that in Fig. 6a. The same argument also holds for oxidized $Ag/SiO_x/Si(100)$ if one assumes a complete desorption of silver and oxide after heating to 900°C. For the oxidized case, traces of both silver and oxide must remain on the surface, since the image contrast observed after heating (Fig. 3e and f) is comparable to neither clean Si(100) (Fig. 6a) nor to oxidized Si(100) (Fig. 1) nor to silver covered Si (100) (Fig. 6c). To our knowledge, the detailed structure of a Shiraki oxide has not yet been investigated. It may be that upon heating, the desorption of the oxide is kinetically hindered by the silver layers so that the oxide remains on the surface.

The conclusion that the remaining traces form a homogeneous layer (on the resolution scale of the PEEM) is supported by the fact that the interfacial structure and hence the electronic structure of the entire surface is changed, as observed in Fig. 4. The silver layer has metallic conductivity and serves as a short circuit of the p–n junctions. The short circuit was measured as a loss of the rectifying behavior of the p–n junction. We assume that the situation is similar in the case of silver deposition on bare silicon. Here, after heating to 900°C, the PEEM images show bright p stripes with dark n regions in between, and most of the three-dimensional islands have disappeared.

4.2. Electronic structure of the Schottky contact and the PEEM contrast

In this section we discuss the relation between the image contrast and the position of the Fermi level at the interface. A quantitative interpretation of the PEEM contrast in terms of the electronic band structure would require a modeling of the space charge layer near the interface and the calculation of the photo yield, which is beyond the scope of this work. Here, we focus on a qualitative interpretation of the relative intensities in the PEEM images for the n- and p-doped regions in terms of the band bending near the surface. The principal arguments have already been laid out in a previous publication [1]. Differently doped areas on a device structure give rise to different photoemission yields when the Fermi level is pinned at the surface by surface states. Due to the pinning, the band bending near the surface depends on the doping, leading to a spatial variation of the effective photo-threshold [1,2]. The attenuation length of 5-eV photons into silicon is known to be approximately 60 Å [26]. The mean free path of the photoemitted electrons is likely to vary rapidly with threshold, but previous estimates have been 12–25 Å [2,27]. These effects limit the depth which might be probed in these experiments. However for the heavily doped p regions, band bending can occur over a comparable scale [27], allowing photoemission from the bulk valence level.

A key to the interpretation is that in our experiments the maximum photon energy barely exceeds the photo-threshold (in the cases where we observe any intensity at all). Under such circumstances, the photo yield is then to a large extent determined by the effective photo-threshold. In the absence of a space charge layer near the surface (i.e. for the flat band condition), the photo-threshold is the

difference between the vacuum level and the valence-band energy and conduction-band energy for p- and n-type doping, respectively (Fig. 8). In this case, the n-doped areas should provide a higher photo yield, as long as the doping is large enough to provide sufficient photoemission from the conduction band. The p-doped areas as well as the transition regions between n- and p-doped regions would appear as dark. In the center of the p-doped stripes the doping level reaches a maximum. There, the acceptor levels and the valence band form a continuum which effectively lowers the photo-threshold. This may explain the increase in the intensity in the center of the p stripes. The photo yield in Fig. 4 can thus be explained assuming a flat-band condition for the $Ag/SiO_x/Si(100)$ system (A) (i.e. the Fermi level is not pinned by interface states after heating to 900°C). Qualitatively, the PEEM images would be also consistent with a small band bending. A more quantitative analysis would require the calculation of the photo yield, as mentioned above.

For the second interfacial system Ag/Si(100)(B) (after heating to 900°C), the brightness of the p stripes compared to the n areas (Figs. 6c and 9) is based on two effects. First, the photo-threshold is reduced due to the low work function of any residual silver ($\phi = 4.8$ eV [24]). The second explanation for the brightness of the p stripes is possibly the strong downward band bending in the p^+ region due to Fermi-level pinning in the lower half of the band gap, which decreases the photo-threshold (Fig. 9). In the n-doped area and in the transition region between n and p, the additional effect of the band bending is removed. Here, the interface states cause a smooth upward bending and the photo-threshold is not effectively lowered. The intensity in the PEEM image in the n-doped region as well as in the transition region may arise only from the reduction of the photo-threshold by the silver overlayer, which is the same regardless of the doping level. Hence, no intensity minimum between p and n is observed.

Finally, we discuss our band model for system (B) with respect to the Schottky barrier height. As mentioned earlier, the Schottky barrier height (SBH) of this system has already been determined for Ag growth at 400–500°C to be of the order of

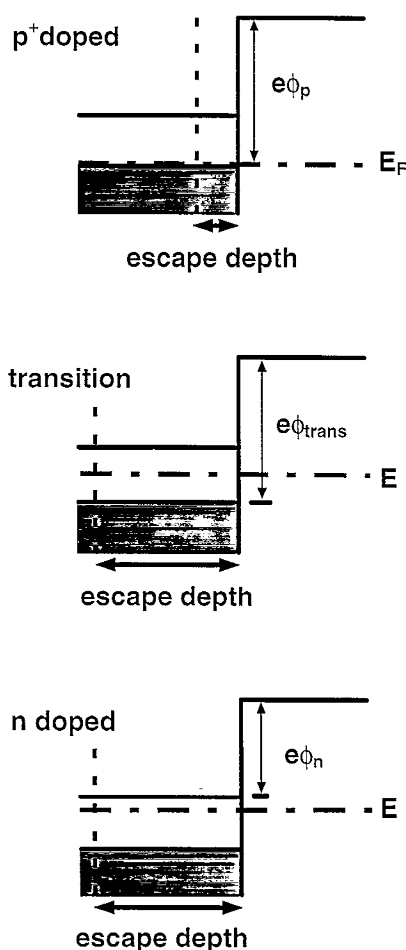

Fig. 8. Band bending model for the metal–semiconductor interface with an intermediate oxide layer after annealing to 900°C. The Fermi level is not pinned by interface states in the band gap, so that there is no band bending at the interface. In the transition region between the n- and p^+-doped stripes and in the p^+-stripe the photo-threshold is given by the distance between the valence-band energy and the vacuum level. The doping level reaches its maximum in the center of the p stripe. There, the photo-threshold is reduced due to the formation of a continuous band between the acceptor levels and the valence band. In the n-doped stripes, the conduction band is effectively occupied by electrons so that the photo-threshold is given by the distance between the conduction-band energy and the vacuum level. The escape depths are larger for the n-doped and the transition regions due to the lower defect density compared to the p^+-doped area. (The escape depths in the figures are not to scale.)

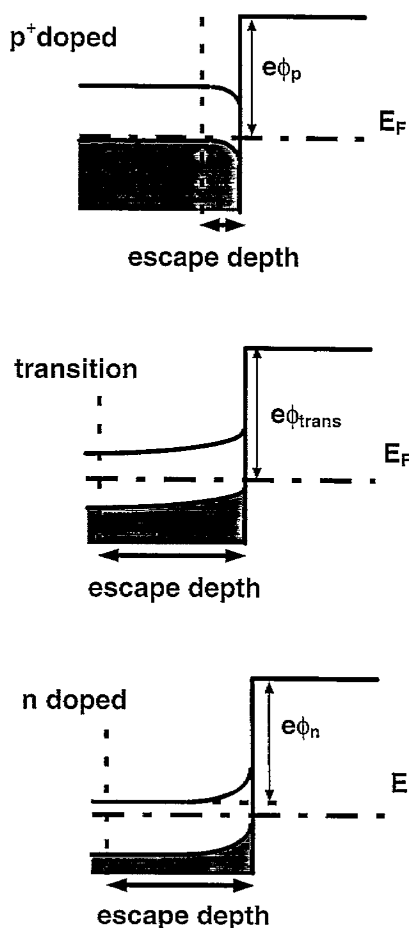

Fig. 9. Band bending model for the direct metal–semiconductor interface after annealing to 900°C. The Fermi level is pinned in the lower half of the band gap by interface states. The pinning of the Fermi level causes a band bending at the interface in the heavily p^+-doped regions. There, the bulk valence-band energy is shifted towards the vacuum level. The photo-threshold for the p^+ stripes is determined by the bulk valence-band energy if the escape depth of electrons is larger than the space charge layer. For both the transition between n- and p^+-doped regions and the n regions, the band bending has the opposite sign to the p^+ regions. Since only a few electrons occupy the conduction band in the n region, the effective photo-threshold is given in the n region as well as in the transition region by the valence-band edge. (The escape depths in the figures are not to scale.)

0.75 eV for light n doping and of the order of 0.4 eV for heavy p doping [17–19]. However, some results differ by tenths of an eV. In this work, silver was deposited at room temperature and then annealed to 900°C. From our band model we can determine the SBH for the light n doping to be higher than half the band gap, which is 1.1 eV for silicon (i.e. SBH>0.5 eV). This value is in agreement with the results presented in Refs. [17–19]. We can also give an estimate for the SBH for heavy p^+ doping, which is smaller than 0.5 eV, which again agrees with earlier publications [17–19].

5. Summary

We have shown that silver deposited on a partially oxidized Si(100) surface induces interface states in the band gap which differ from the states on the oxidized surface without deposition of Ag, as well as from the interface states without an oxide layer between silver and the Si(100) surface. We have shown that in the latter case the Fermi level must be pinned in the lower half of the band gap. In the case of a partially oxidized interface, the Fermi level is not pinned by interface states so that no band bending is observed. At present, the structure and composition of the metal oxide–semiconductor interface system are not understood. On the scale of the resolution of PEEM, the surface structure with and without the oxide layer appears similar. In both cases, a homogeneous metallic overlayer is formed and the diffusivity of silver islands on this layer is high.

It should be emphasized that while the models suggested above provide an interpretation of the qualitative features of the observed contrast, other more complex scenarios cannot be excluded. A full theoretical analysis as well as further studies which should involve a systematic variation of the doping levels should eventually bring about the potential for a quantitative determination of the position of the Fermi level at the metal–semiconductor interface. This could establish PEEM as a novel tool for the quantitative investigation of the electronic structure of interfaces, with the capability of observations in real time.

Acknowledgements

This work has been carried out with support from the Laboratory for Physical Science. We are

grateful to R. Wilson for the use of the PEEM, to A. Fernandez for the preparation of the samples and for many useful discussions, and to H. Shibata and H. Kan for their contributions. We also gratefully acknowledge helpful discussions with H. Ibach. Support for the fabrication and initial characterization of the devices was provided by the NSF-FAW (DMR-90-2345) and the Cornell Nanofabrication Facility. One of the authors (M.G.) gratefully acknowledges the support of the Alexander von Humboldt Stiftung, Germany, and the University of Maryland NSF-MRSEC (DMR 96-32521).

References

[1] M. Giesen, R.J. Phaneuf, E.D. Williams, T.L. Einstein, H. Ibach, Appl. Phys. A 64 (1997) 423.
[2] F.G. Allen, G.W. Gobeli, Phys. Rev. 127 (1962) 150.
[3] G. Le Lay, Surf. Sci. 132 (1983) 169.
[4] K. Spiegel, Surf. Sci. 7 (1967) 125.
[5] J.A. Venables, P. Akhter, J. Derrien, Surf. Sci. 95 (1980) 411.
[6] G. Le Lay, M. Manneville, R. Kern, Surf. Sci. 72 (1978) 405.
[7] M. Saitoh, F. Shoji, K. Oura, T. Hanawa, Surf. Sci. 112 (1981) 306.
[8] M. Hanbücken, H. Neddermeyer, P. Rupieper, Thin Solid Films 90 (1982) 37.
[9] M. Hanbücken, H. Neddermeyer, Surf. Sci. 114 (1982) 563.
[10] M. Hanbücken, M. Futamoto, J.A. Venables, Surf. Sci. 147 (1984) 433.
[11] A. Samsavar, E.S. Hirschhorn, F.M. Leibsle, T.-C. Chiang, Rev. Lett. 63 (1989) 2830.
[12] A. Brodde, D. Badt, S. Tosch, H. Neddermeyer, J. Vac. Sci. Technol. A 8 (1990) 251.
[13] N. Doraiswamy, G. Jayaram, L.D. Marks, Phys. Rev. B 51 (1995) 10167.
[14] Y. Kimura, K. Takayanagi, Surf. Sci. 276 (1992) 166.
[15] F.K. LeGoues, M. Liehr, M. Renier, W. Krakow, Philos. Mag. B 57 (1988) 179.
[16] A. Samsavar, T. Miller, T.-C. Chiang, Phys. Rev. B 38 (1988) 9889.
[17] H.H. Weitering, J.P. Sullivan, R.J. Carolissen, R. Pérez-Sandoz, W.R. Graham, R.T. Tung, Appl. Surf. Sci. 70/71 (1992) 422.
[18] J. Tersoff, Phys. Rev. Lett. 52 (1984) 465.
[19] Y. Borensztein, R. Alameh, M. Roy, Phys. Rev. B 48 (1993) 14737.
[20] J.C. Glueckstein, M.M.R. Evans, J. Nogami, Phys. Rev. B 54 (1996) 11067.
[21] T. Ichinokawa, C. Haginoya, D. Inoue, H. Itoh, J. Phys. A 5 (1993) 405.
[22] A. Fernandez, in preparation.
[23] A. Ishizaki, Y. Shiraki, J. Electrochem. Soc. 133 (1986) 666.
[24] C. Kittel, Introduction to Solid State Physics, 2nd ed., Wiley, New York, 1961, p. 267.
[25] M. Hildner, R.J. Phaneuf, E.D. Williams, in preparation.
[26] H.R. Philipp, E.A. Taft, Phys. Rev. 120 (1960) 37.
[27] C. Sebenne, D. Bolmont, G. Guichar, M. Bakanski, Phys. Rev. B 12 (1975) 3280.